

Supplementary Information for Regions of Interest as nodes of dynamic functional brain networks

Elisa Ryyppö¹, Enrico Glerean², Elvira Brattico³, Jari Saramäki¹, and Onerva Korhonen^{1,2,*}

¹Department of Computer Science, School of Science, Aalto University, Espoo, Finland

²Department of Neuroscience and Biomedical Engineering, School of Science, Aalto University, Espoo, Finland

³Center for Music in the Brain, Department of Clinical Medicine, Aarhus University, & The Royal Academy of Music Aarhus/Aalborg, Denmark

*Corresponding author: Onerva Korhonen, email:
onerva.korhonen@aalto.fi

1 Supplementary methods

1.1 Selection of time window length

For constructing time-dependent functional networks from fMRI data, we needed to divide the measurement time series into time windows. We used sliding windows that were 80 samples (160s) long; overlap between two consecutive windows was 50%. Selecting the length of the time window required compromising. On the one hand, we wanted to have as many time windows as possible in order to maximize the number of data points in the analysis of temporal variation in spatial consistency. On the other hand, we wanted to avoid possible distortion in Pearson correlation coefficient and, consecutively, in spatial consistency caused by too short time windows.

To find the optimal window length, we used data of one subject from the in-house dataset. For this subject, we placed a time window at the beginning of the measurement time series. The length of this time window varied between $l = 5$ and $l = 195$ samples with steps of 5 samples. Length of the last time window was comparable to the length of

the entire time series (244 samples). In each of the time windows, we calculated spatial consistency of each ROI. Then, we investigated the mean spatial consistency over ROIs.

First, mean spatial consistency increased as a function of window length, showing that short window lengths may have distorted values of spatial consistency. At larger window lengths, spatial consistency saturated and stayed stable when the window length approached the length of the entire time series. The window length used in the present study, 80 samples, was picked from the beginning of the saturation area. Similar lengths of time windows have been used in the literature ([Bassett et al., 2011, 2013](#)).

We did the above-described investigation using both non-overlapping windows and sliding windows with 50% overlap. Since at window length of 80 samples there was no visible difference in mean spatial consistency between the window types, we decided to use sliding windows to maximize the overall number of windows.

1.2 Selection of the closest neighborhood size

Network turnover quantifies the tendency of ROI's closest neighborhood to change in time. The closest neighborhood is defined as a set of neighbors most strongly connected to the ROI. To determine an optimal size for the closest neighborhood, we calculated for all subjects of the in-house dataset the mean Jaccard index over time window pairs using a set of closest neighborhood sizes ranging from 5 to 195 with steps of 5. For each ROI, we averaged the Jaccard indices over subjects.

On average, the Jaccard index increased with the increasing closest neighborhood size. However, behavior of all ROIs was not similar. Instead, for some ROIs the Jaccard index decreased with the increasing closest neighborhood size when the neighborhood size was small, whereas for other ROIs the Jaccard index increased with the increasing closest neighborhood size over all neighborhood sizes. At larger closest neighborhood sizes, the differences between ROIs disappeared and the Jaccard index increased with increasing closest neighborhood size for all ROIs. The closest neighborhood size used in the present study, 35, was selected from the area where the differences between ROIs disappear and the monotonic increase of the Jaccard index begins.

1.3 ABIDE data

In order to investigate how our results generalize for other datasets, we repeated all analyses for a secondary, independent dataset. This dataset was collected as a part of the Autism Brain Imaging Data Exchange (ABIDE) initiative ([Di Martino et al., 2014](#)). We refer to this dataset as the ABIDE data.

Subjects

The ABIDE dataset included resting-state data of 31 healthy subjects that were measured at NYU Langone Medical Center. During the preprocessing and quality control, 3 of these subjects were excluded due to exceptional amount of motion. This left for further analysis

28 subjects (7 female, 21 male, age 29.9 ± 3.8 , mean \pm SD). Based on Structured Clinical Interview for DSM-IV-TR Axis-I Disorders, Non-patient Edition (SCID-I/NP) and Adult ADHD Clinical Diagnostic Scale (ACDS) questionnaires, the subjects did not suffer from autism spectrum disorders. The ABIDE IDs of the subjects were 51057, 51058, 51059, 51060, 51061, 51062, 51063, 51066, 51067, 51112, 51113, 51114, 51115, 51116, 51117, 51118, 51119, 51130, 51131, 51146, 51147, 51148, 51149, 51151, 51152, 51153, 51154, and 51155.

Data acquisition

Subjects were measured with a 3T Allegra MRI device (Siemens Medical Solutions, NJ, USA). Structural MR images were acquired with a T1-weighted MP-RAGE sequence with voxel size of $1.3 \times 1.0 \times 1.3$ mm 3 . Resting-state fMRI data were measured as a T2*-weighted EPI-sequence with the following parameters: TR = 2.0s, TE = 15ms, flip angle = 90°, voxel size = $3.0 \times 3.0 \times 5$ mm 3 , matrix size = $80 \times 80 \times 33$, FOV = 240×240 mm 2 . The length of the data was 6 minutes (180 time points). During the measurement, subjects were instructed to relax with their eyes open, while a white cross-hair against a black background was projected on a screen. However, some subjects may have closed their eyes regardless of instructions.

Preprocessing and analyses

The ABIDE dataset went through the same preprocessing and analyses as the in-house dataset (see the main text for details).

We analysed the ABIDE dataset using 245 ROIs from the Brainnetome atlas. The size of these ROIs, measured as the number of voxels, varied between 8 and 1148 with mean being 362.7, SD being 235.9, and median being 299. Note that location of one ROI, right thalamus (8_8) did not overlap over all subjects of the ABIDE dataset, and this ROI was therefore excluded from the analysis.

2 Supplementary results

2.1 In-house data analysed with AAL and HO atlases

For investigating the time-dependent behavior of functional homogeneity and changes in local network structure in our in-house dataset, we used three different parcellations of the brain: the connectivity-based Brainnetome atlas as well as anatomical Automated Anatomical Labeling (AAL) and HarvardOxford (HO) atlases. In the main article, we have reported the results obtained using Brainnetome. Using AAL and HO gave very similar results. For detailed discussion of the results, the reader is referred to the Results section of the main article.

Functional homogeneity, measured in terms of static spatial consistency, varies a lot between ROIs of Brainnetome, AAL, and HO, as we have reported in the main article (see

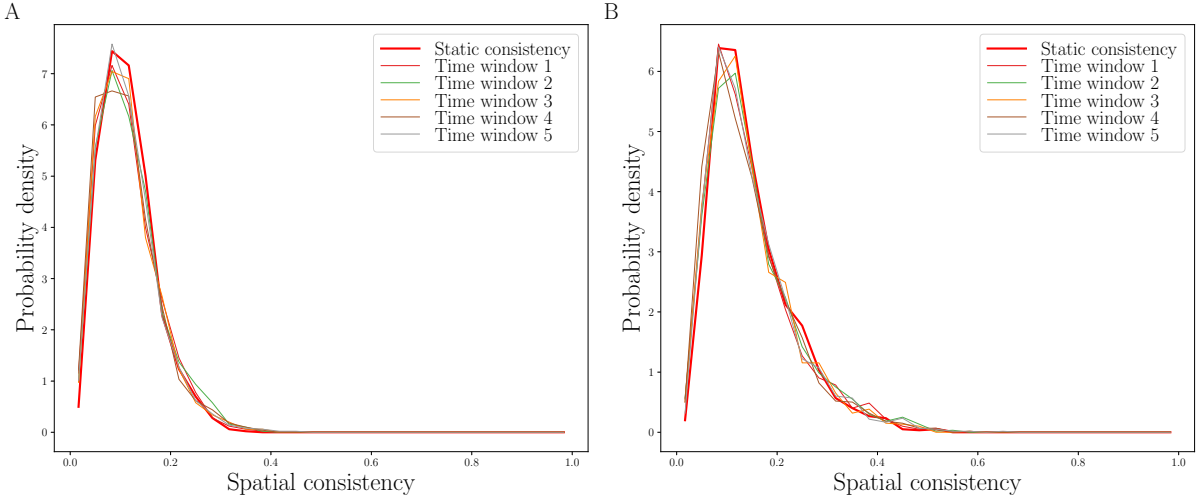


Figure S1: Distributions of spatial consistency calculated separately for five time windows of 80 samples for A) AAL and B) HO ROIs. There is no visible difference between the distributions calculated for different time windows. All distributions have been calculated from pooled data of 13 subjects.

Fig. 1). For investigating the time-dependent behavior of spatial consistency, we divided the data into five time windows. There is no visible difference between distributions of spatial consistency calculated in different time windows for either AAL or HO (Fig. S1). In both AAL and HO, static spatial consistency is negatively correlated with ROI size (AAL: $r = -0.32$, $p = 4.13 \times 10^{-4}$; HO: $r = -0.33$, $p = 8.62 \times 10^{-5}$; Fig. S6A, D).

Although the pooled distributions of spatial consistency do not differ between time windows, there are significant relative changes in the spatial consistency of single ROIs (Fig. S2A, Fig. S3A). This leads to a nonuniform spatial distribution of spatiotemporal consistency that quantifies the changes in spatial consistency (Fig. S2B, Fig. S3B). The AAL and HO ROIs with the highest and lowest spatiotemporal consistency are listed in the main article. There is no significant correlation between ROI size and spatiotemporal consistency in either AAL or HO (AAL: $r = 0.16$, $p = 0.0963$; HO: $r = -0.025$, $p = 0.770$; Fig. S6B, E).

Changes in the local network structure around AAL and HO ROIs are visible as significant neighborhood turnover between subsequent time windows (Fig. S4A, Fig. S5A). This turnover is anatomically nonuniformly distributed and shows strong spatial correlation (Fig. S4B, Fig. S5B). The AAL and HO ROIs with the highest and lowest values of network turnover are listed in the main article. In particular, subcortical and cerebellar areas tend to have high network turnover. Network turnover is negatively correlated with ROI size in both AAL and HO (AAL: $r = -0.42$, $p \ll 10^{-5}$; HO: $r = -0.30$, $p = 4.02 \times 10^{-4}$; Fig. S6C, F).

Spatiotemporal consistency and network turnover are negatively correlated in both

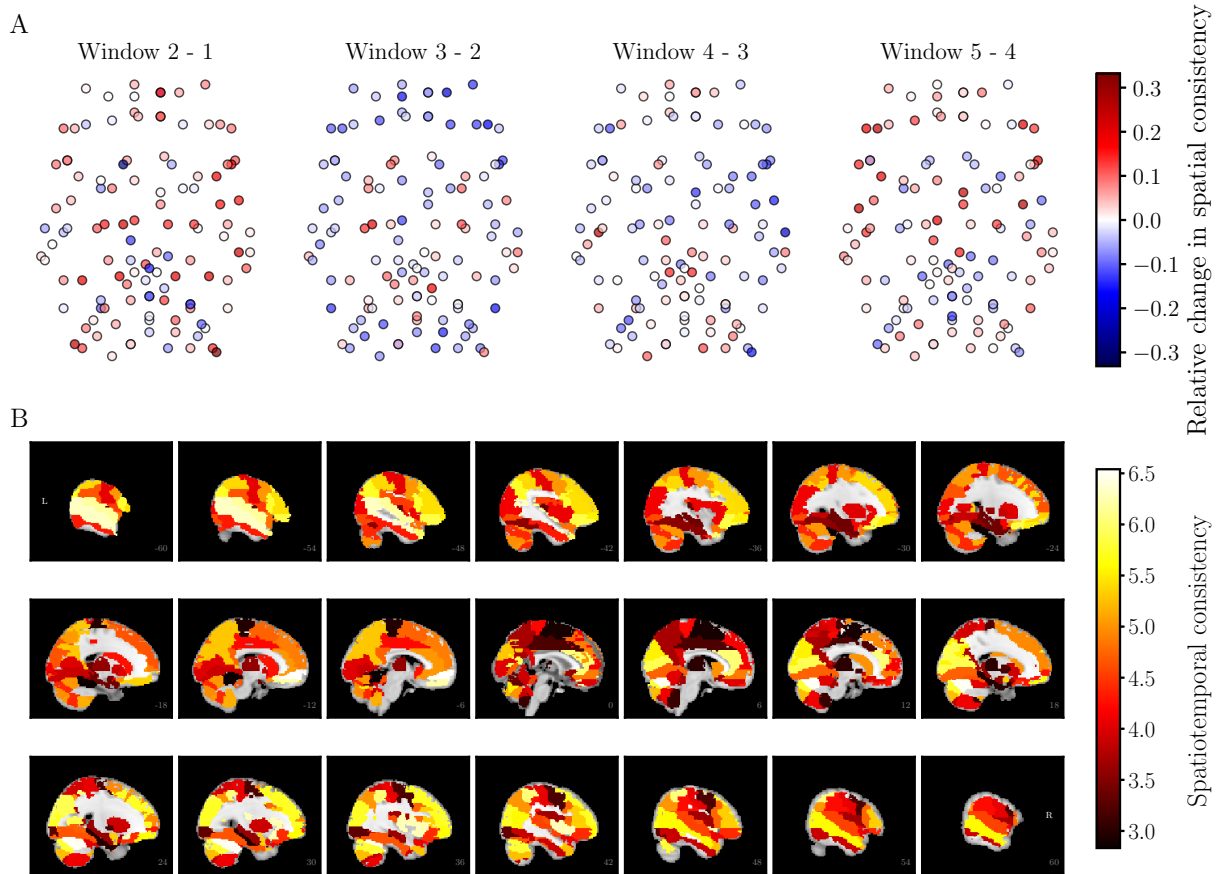


Figure S2: Spatial consistency changes in time. A) Relative changes in spatial consistency between subsequent time windows in the AAL atlas. The changes are non-randomly distributed in time and show strong spatial correlation, similarly as in the Brainnetome atlas (see Fig. 2 of the main article). The location of nodes is determined by a two-dimensional projection of the anatomical coordinates of ROI centroids similarly as in Fig. 2 of the main article. The visualization follows the neurological convention. B) The spatiotemporal consistency of AAL ROIs on brain surface. Spatiotemporal consistency has a non-uniform anatomical distribution and shows strong spatial correlation. All results are averaged over 13 subjects. Grayscale areas are not included in the present study (white matter).

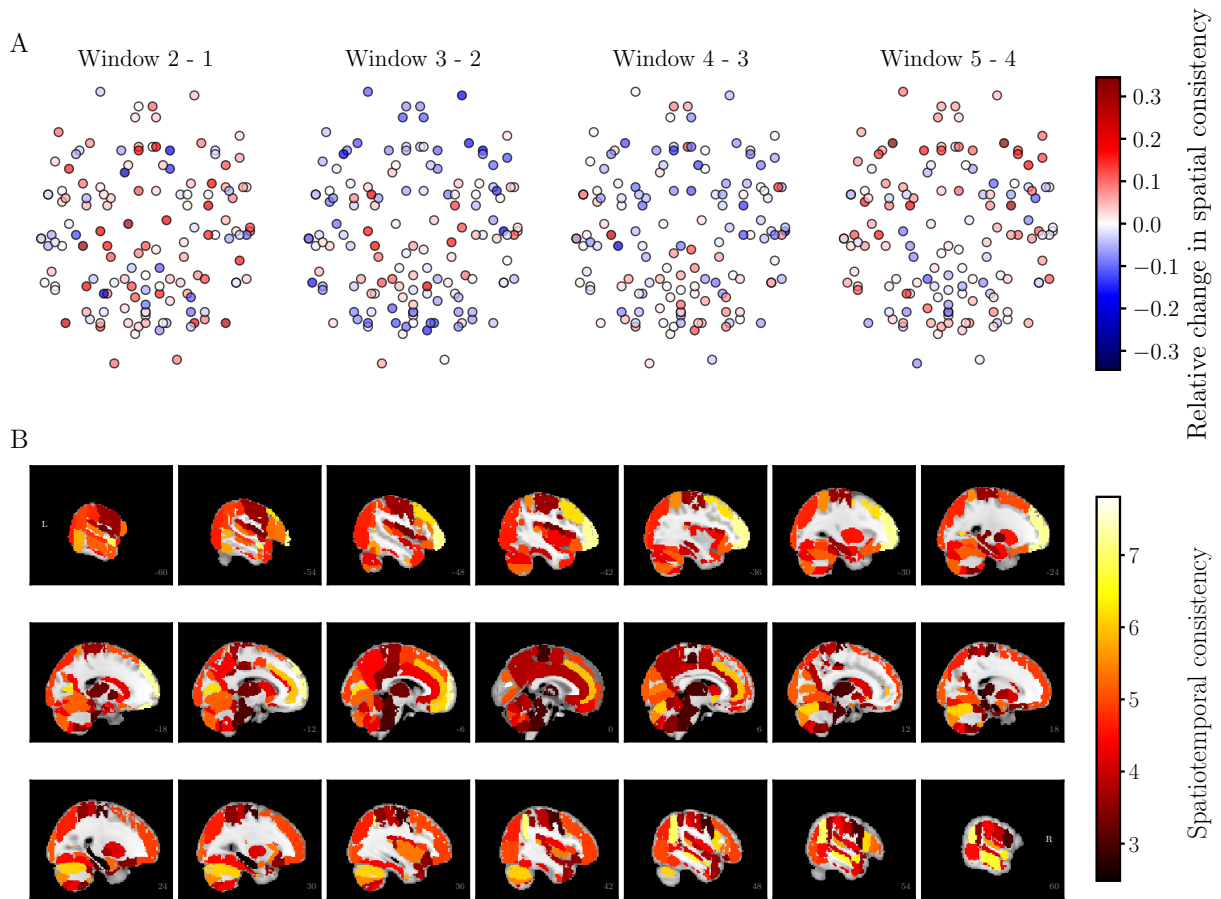


Figure S3: Time-dependent behavior of spatial consistency in HO atlas. A) Relative changes in spatial consistency between subsequent time windows. B) Spatiotemporal consistency on brain surface. All results are averaged over 13 subjects. For further details, see Fig. S2 and Fig. 2 of the main article.

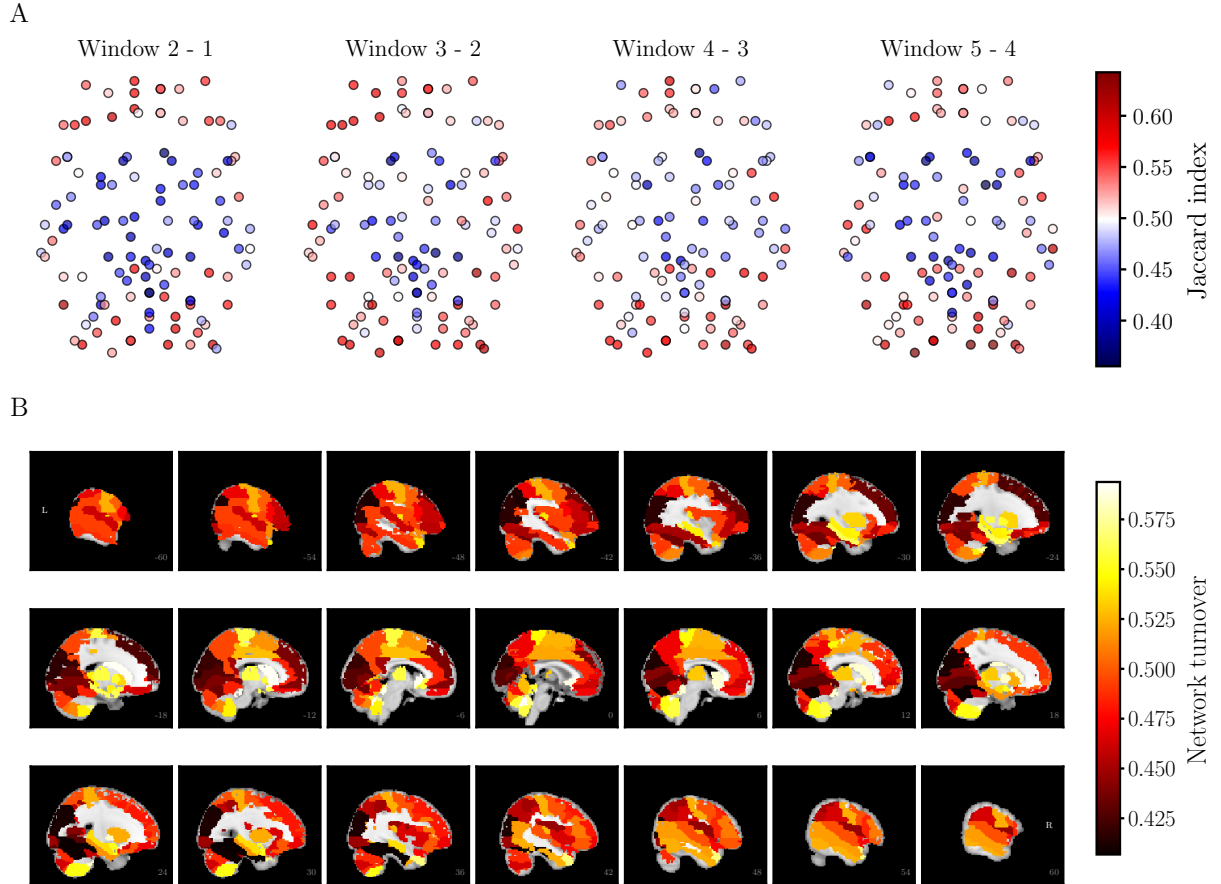


Figure S4: Strong neighborhood turnover takes place in dynamic functional brain networks. A) The Jaccard index between subsequent time windows in the AAL atlas. Values of the Jaccard index are spatially nonuniformly distributed and show strong spatial correlation, similarly as in the Brainnetome atlas (see Fig. 3 of the main article). Node locations are as in Fig. S2. B) Network turnover of AAL ROIs on brain surface. All results are averaged over 13 subjects.

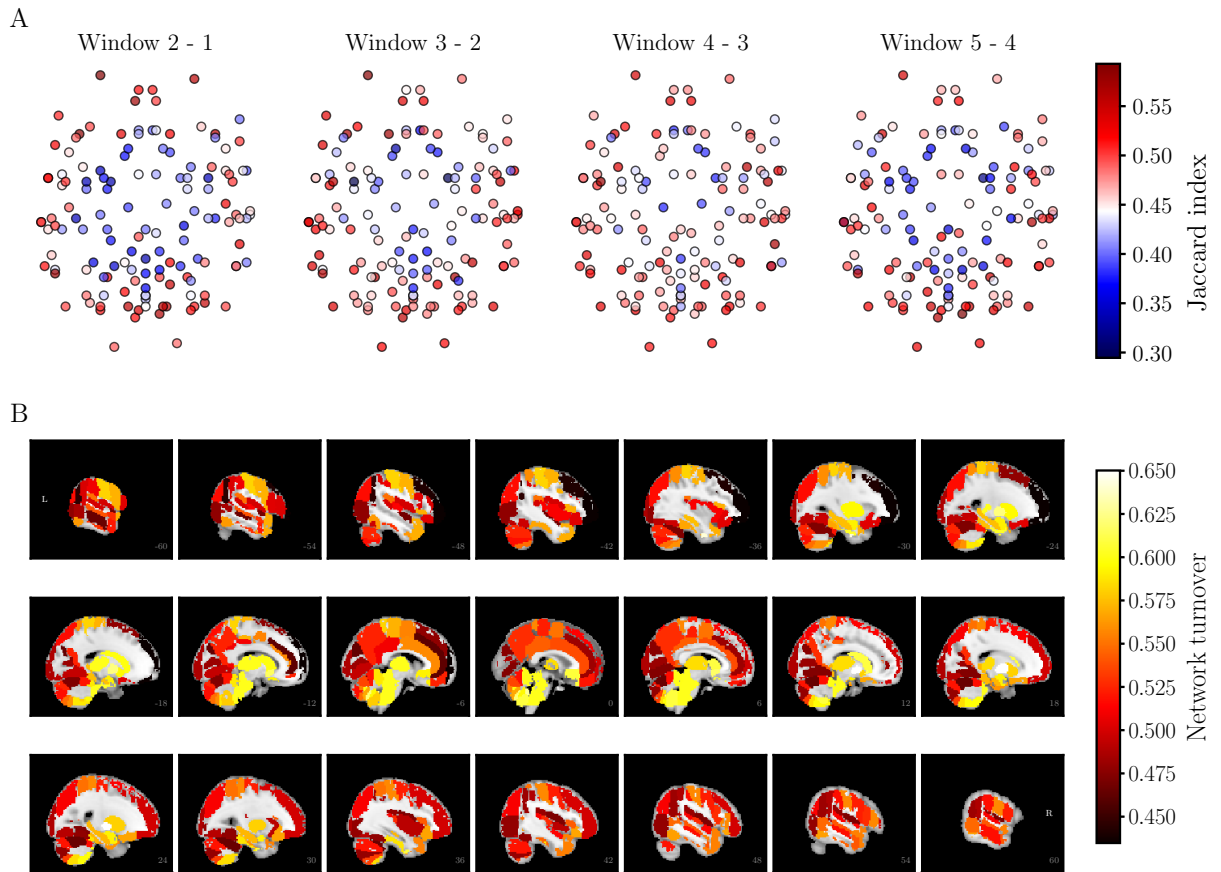


Figure S5: Changes in local network structure in the HO atlas. A) The Jaccard index between subsequent time windows. B) Network turnover on brain surface. All results are averaged over 13 subjects. For further details, see Fig. S4 and Fig. 3 of the main article.

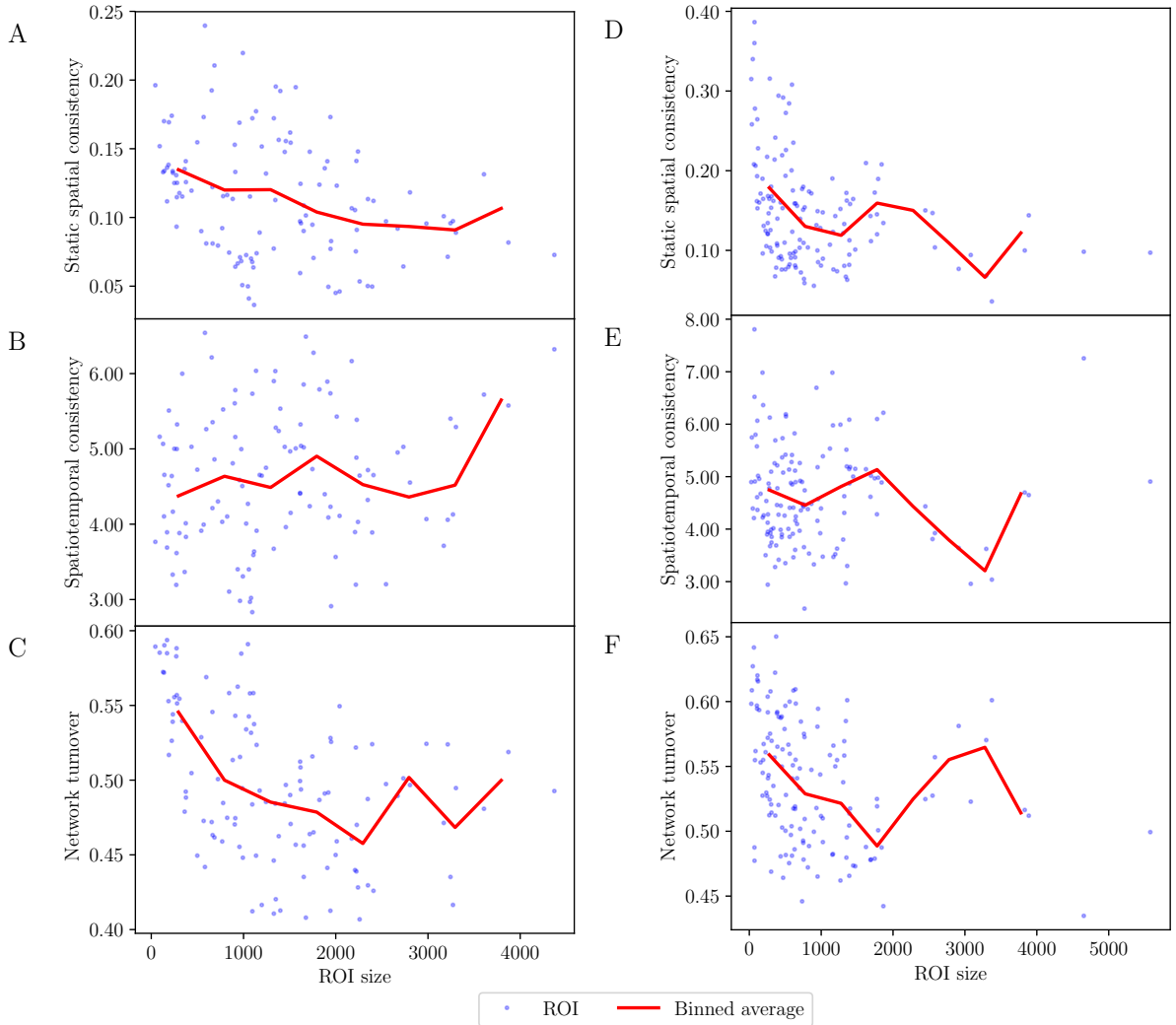


Figure S6: Relationship between sizes of AAL (left column) and HO (right column) ROIs and their spatial and spatiotemporal consistency and network turnover. There is a weak negative correlation between static spatial consistency and ROI size in both AAL (A) and HO (D). Spatiotemporal consistency does not correlate with ROI size either in AAL (B) or in HO (E). Network turnover is negatively correlated with ROI size in both AAL (C) and HO (F). All results are averages over 13 subjects. Solid red lines show bin averages, binning as in Fig. 4 of the main article.

AAL and HO, similarly as in Brainnetome (AAL: $r = -0.38$, $p = 2.08 \times 10^{-5}$; HO: $r = -0.44$, $p \ll 10^{-5}$; Fig. S7A, Fig. S8A). ROIs with high static spatial consistency tend to have high spatiotemporal consistency and low network turnover in both AAL and HO (Fig. S7B, Fig. S8B). In AAL, ROIs with high spatiotemporal consistency and low network turnover tend to be larger than ROIs with low spatiotemporal consistency and high network turnover, although the connection is not as clear as for Brainnetome ROIs (Fig. S7C). In HO, such connection is not visible (Fig. S8C). Bearing in mind the lack of correlation between the size of HO ROIs and their spatiotemporal consistency and the weak correlation between size of HO ROIs and their network turnover, this result should not be surprising.

We used principal component analysis (PCA) to find two groups of extreme ROIs: five ROIs with high spatiotemporal consistency and low network turnover and five ROIs with low spatiotemporal consistency and high network turnover (Fig. S9, Fig. S10). In both AAL and HO, ROIs of the first extreme group are located in the cortex, whereas the second extreme group contains subcortical and cerebellar areas. For further methodological details as well as the identity of the extreme ROIs, the reader is referred to the main article.

From both AAL and HO, we selected four extreme ROIs for further investigation. The selected AAL ROIs were orbital part of left middle frontal gyrus, right superior occipital gyrus, right olfactory cortex, and right globus pallidus. From HO, we selected left and right supracalcarine cortex, left globus pallidus, and right hippocampus. To investigate the internal connectivity of these ROIs, we calculated the voxel-level intra-ROI correlation matrices (Fig. S11). Rich, time-dependent connectivity structure is visible in all these ROIs, similarly as in Brainnetome ROIs. Although the overall voxel-level correlation is higher in ROIs with high spatiotemporal consistency, the correlations are not uniformly distributed. Instead, voxels are divided into several internally highly correlated subareas in all investigated ROIs. The time-dependent changes in the internal connectivity structure do not depend on the spatiotemporal consistency neither.

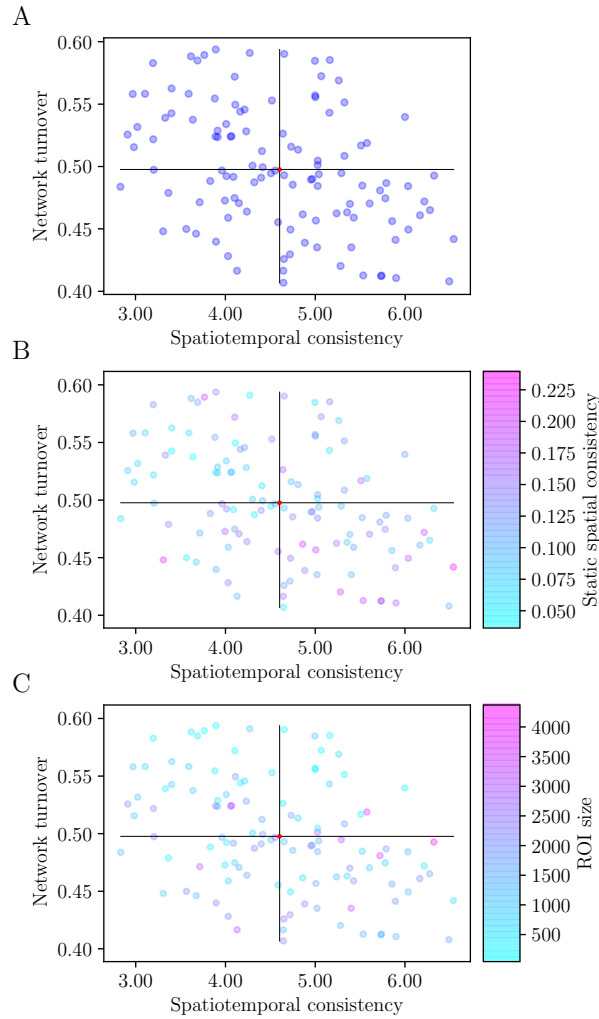


Figure S7: Relationship between static spatial consistency, spatiotemporal consistency, and network turnover in the AAL atlas. A) Spatiotemporal consistency is negatively correlated with network turnover, similarly as in the Brainnetome atlas (see Fig. 5 of the main article). B) ROIs with the highest static spatial consistency tend to have also the highest spatiotemporal consistency and the lowest network turnover. C) ROIs with high spatiotemporal consistency and low network turnover tend to be larger than ROIs with small spatiotemporal consistency and high network turnover. All results are averages over 13 subjects.

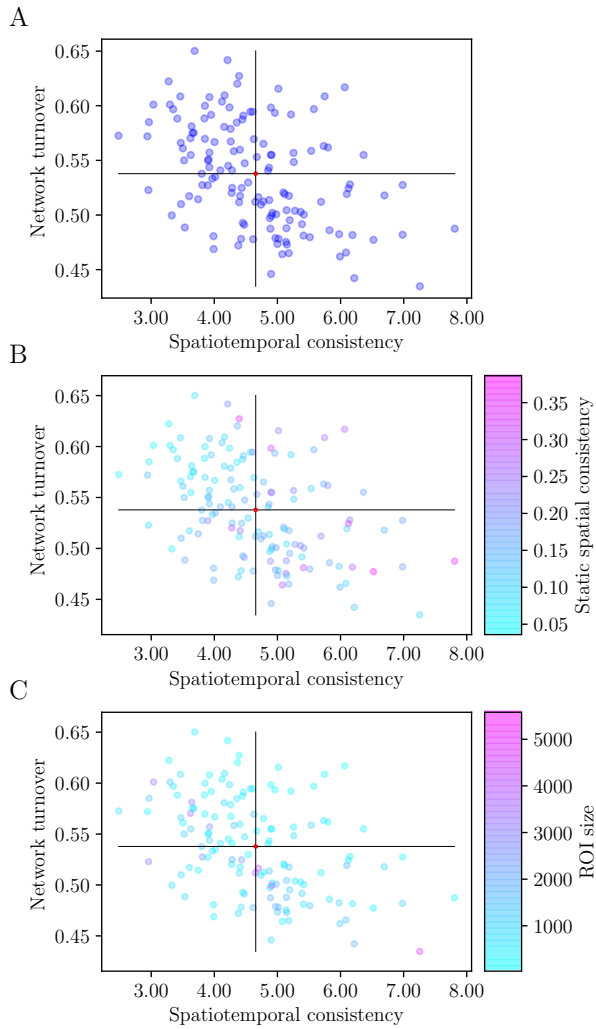


Figure S8: Relationship between static spatial consistency, spatiotemporal consistency, and network turnover in the HO atlas. A) Spatiotemporal consistency correlates negatively with network turnover. B) ROIs with the highest static spatial consistency also have the highest spatiotemporal consistency and lowest network turnover. C) No clear connection is visible between ROI size, spatiotemporal consistency, and network turnover. All results are averages over 13 subjects.

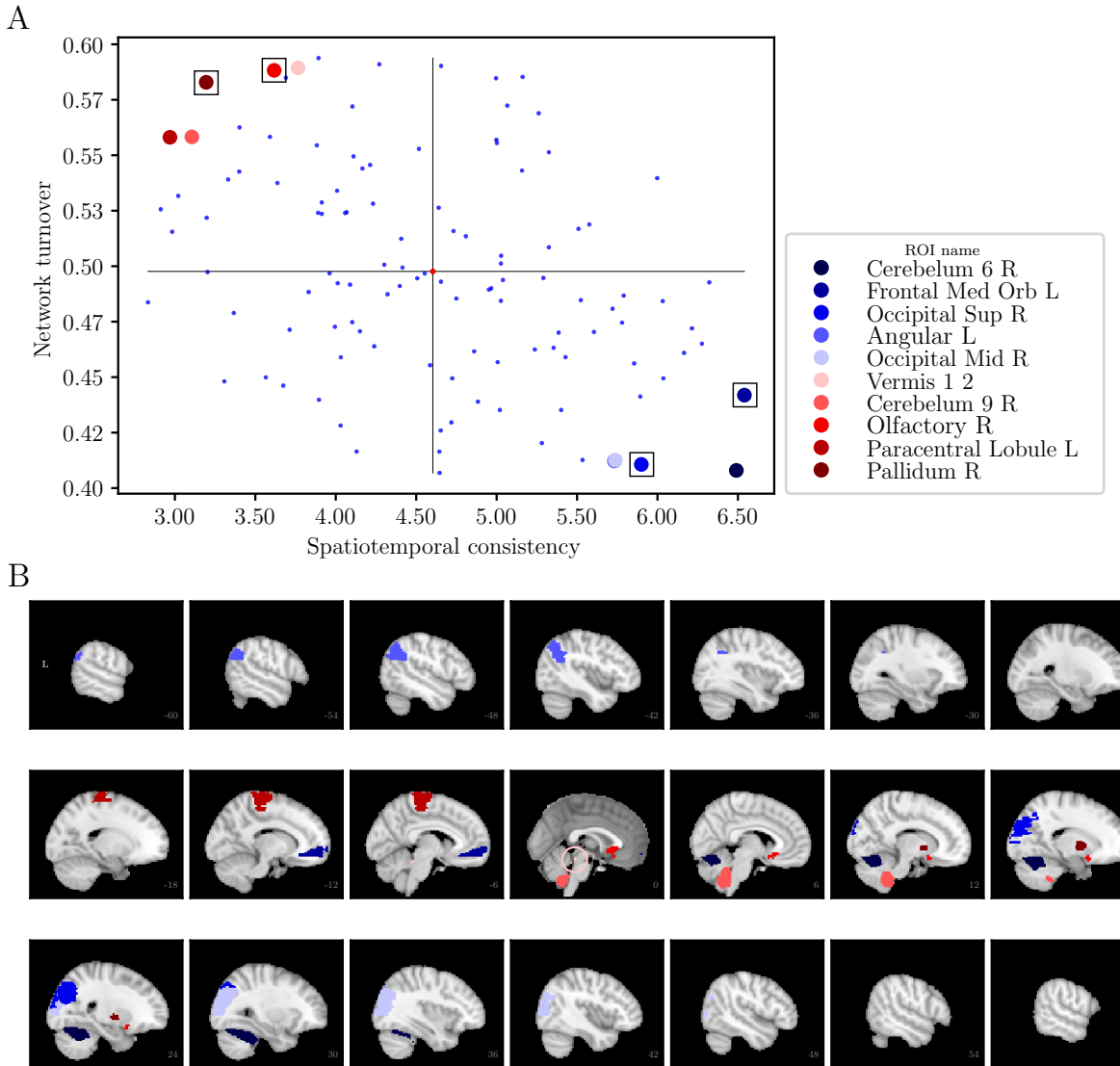


Figure S9: Extreme groups of ROIs in terms of spatiotemporal consistency and network turnover in the AAL atlas. A) Location of the extreme ROIs in the space spanned by spatiotemporal consistency and network turnover. Blue ROIs have high network turnover and low spatiotemporal consistency, whereas red ROIs have low network turnover and high spatiotemporal consistency. For further details, see the main article. For ROIs marked with a square, voxel-level intra-ROI correlation matrices are presented in Fig. S11. B) Anatomical location of the ROIs of the extreme groups. L: left, R: right, Med: medial, Orb: orbitofrontal, Sup: superior, Mid: middle.

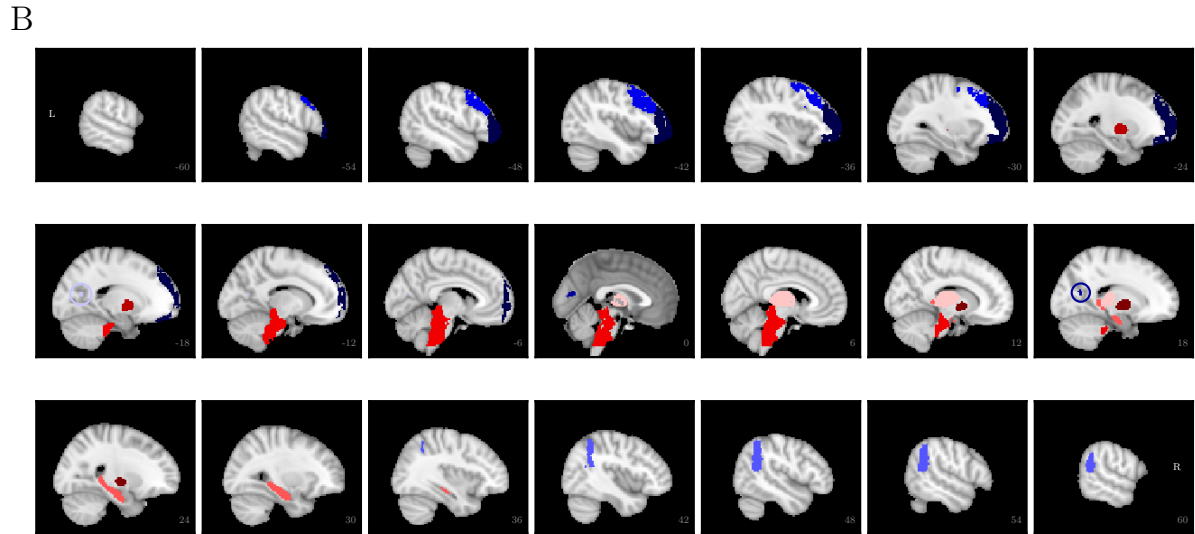
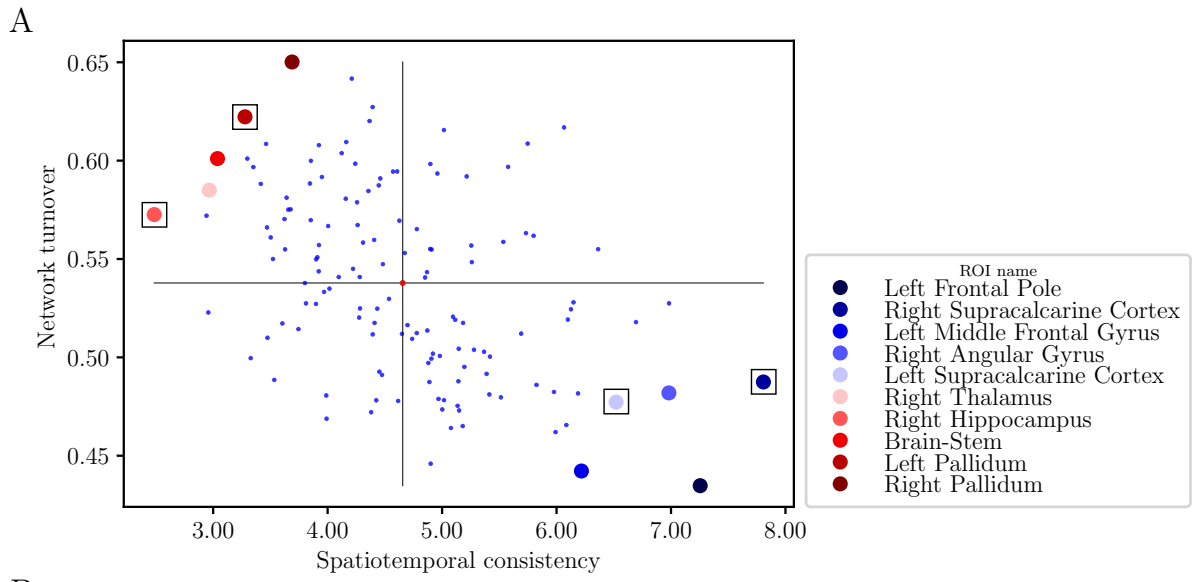


Figure S10: Extreme groups of ROIs in the HO atlas. A) Location of the extreme ROIs in the space spanned by spatiotemporal consistency and network turnover. For further details, see Fig. S9. B) Anatomical location of the extreme ROIs.

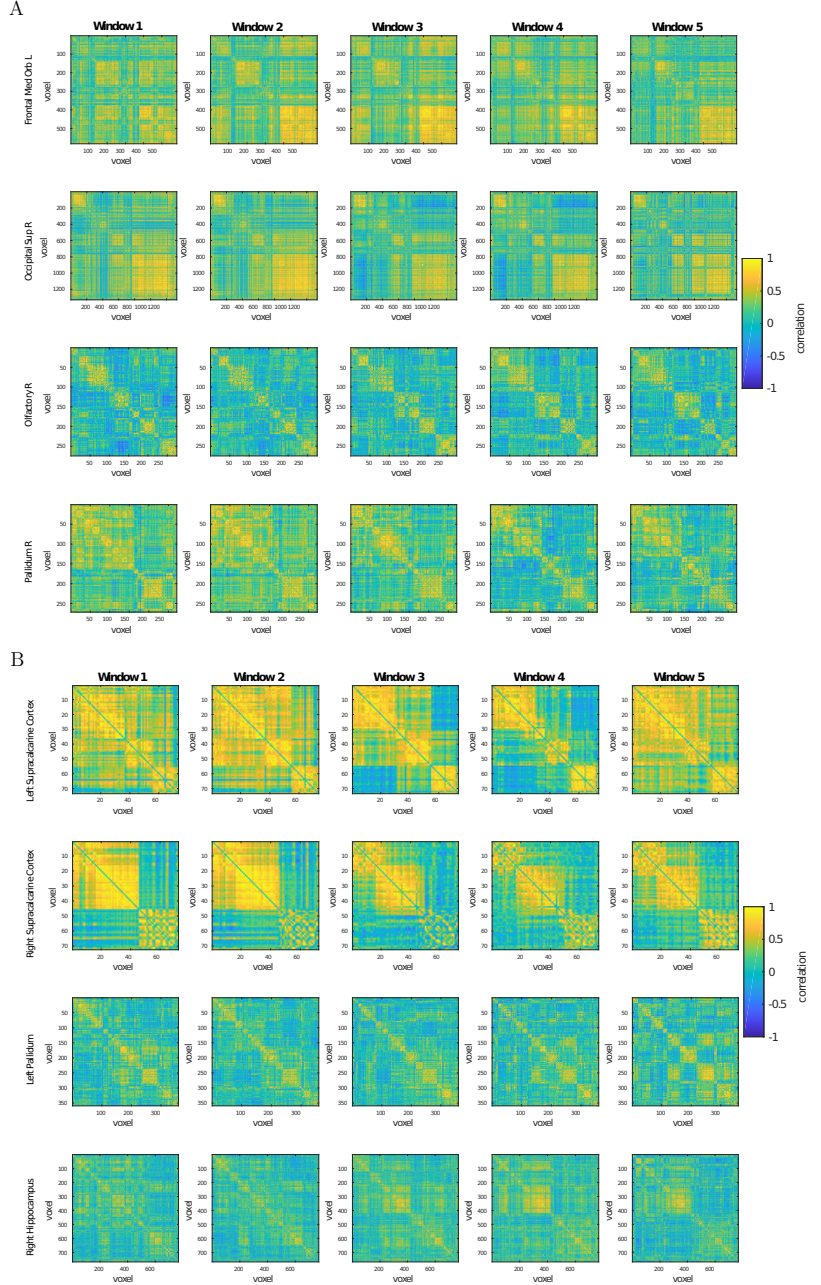


Figure S11: Internal connectivity of ROIs in AAL (A) and HO (B) atlases visualized in terms of intra-ROI voxel-level correlation matrices. For both atlases, the upper two rows display correlation matrices for ROIs with high spatiotemporal consistency and low network turnover (the red extreme group) and two lower rows matrices for ROIs with low spatiotemporal consistency and high network turnover (blue extreme group). For further details, see Fig. 7 of the main article.

2.2 ABIDE data

In order to ensure that the results are not explained by any specific feature of our in-house dataset, we repeated all analyses for a secondary, independent dataset, the ABIDE data. Results obtained using the ABIDE data were very similar to those obtained using the in-house data. Therefore, the results are reported here only briefly and the reader is referred to the main article for a more detailed discussion.

Although the maximum static spatial consistency is relatively high ($\phi_{spatial} = 0.761$), the distribution of static spatial consistency is broad and peaks at a low value ($\phi_{spatial} = 0.15$) (Fig. S12). There is a weak negative correlation between the size of a ROI and its static spatial consistency ($r = -0.21$, $p = 9.90 \times 10^{-4}$; Fig. S15A).

There is no visible difference between distributions of spatial consistency calculated in different time windows (Fig. S12). At the level of single ROIs, however, spatial consistency changes between subsequent time windows, the largest relative change being around 30% (Fig. S13A). These changes lead to an anatomically non-random distribution of spatiotemporal consistency (Fig. S13B), similarly as in the in-house data. The Brainnetome ROIs that have the highest mean spatiotemporal consistency are left precuneus (4_1), left thalamus (8_7 and 8_3), right cuneus (5_3), and right parahippocampal gyrus (6_4). ROIs with the lowest mean spatiotemporal consistency are left precentral gyrus (6_4), right postcentral gyrus (4_4), right striatum (6_1), right thalamus (8_2), and left parahippocampal gyrus (6_3). There is no significant correlation between ROI size and spatiotemporal consistency ($r = 0.039$, $p = 0.544$; Fig. S15B).

Visible turnover takes place in the closest neighborhoods of nodes in the ABIDE data (Fig. S14A). Network turnover is anatomically nonuniformly distributed and shows strong spatial correlation (Fig. S14B). ROIs with the highest mean network turnover are right superior parietal lobule (5_3), left hippocampus (2_2), left precentral gyrus (6_3), left parahippocampal gyrus (6_5), and left inferior temporal gyrus (7_3). ROIs with the lowest mean network turnover include right cuneus (5_5), right precuneus (4_3), left superior occipital gyrus (2_1), left occipital gyrus (4_1), and right inferior parietal lobule (6_4). Similarly as in the in-house data, the ROIs with the highest network turnover are relatively small subcortical areas. There is a significant negative correlation ($r = -0.59$, $p \ll 10^{-5}$) between the size of a ROI and its network turnover (Fig. S15C).

Next, we investigated the relationship between spatiotemporal consistency and network turnover. In the ABIDE data, spatiotemporal consistency of ROIs varies between subjects more than in our in-house data. Because of this, the mean spatiotemporal consistency over subjects was, for some ROIs, exceptionally high. These outlier ROIs were clearly caused by very high values of spatiotemporal consistency in single subjects: when median over subjects was calculated instead of mean, no outlier ROIs were present. Therefore, we used median instead of mean in the analysis of the ABIDE data.

Spatiotemporal consistency and network turnover are negatively correlated ($r = -0.20$, $p = 1.92 \times 10^{-3}$; Fig. S16A). ROIs with the highest static spatial consistency tend to have also high spatiotemporal consistency and low network turnover, similarly as in the in-house data (Fig. S16B). These ROIs also tend to be larger than ROIs with low spatiotemporal

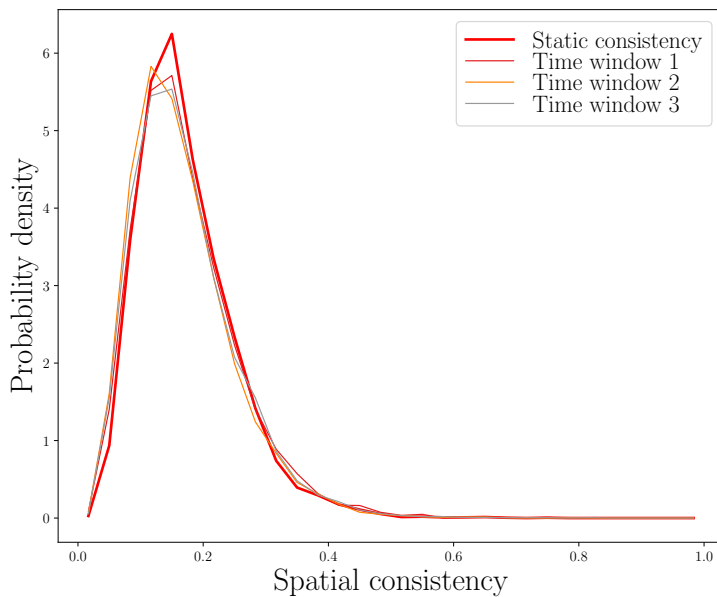


Figure S12: Functional homogeneity varies across ROIs in ABIDE data. Distribution of static spatial consistency (thick red line) and distributions of spatial consistency calculated separately in each of the three time windows of 80 samples. There is no visible difference between the distributions. In the ABIDE data, the time series are shorter than in the in-house data, which leads to a smaller number of time windows. All distributions have been calculated from pooled data of 28 subjects.

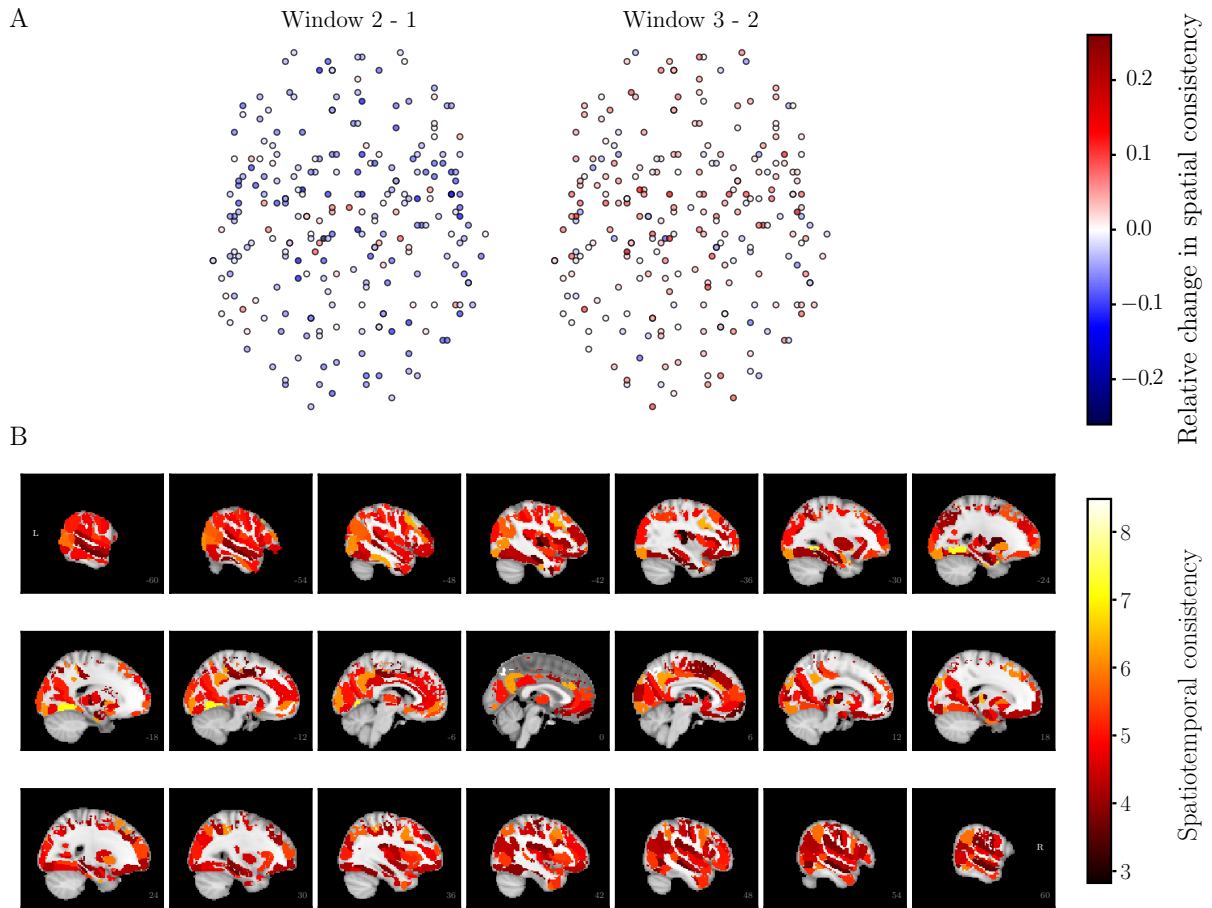


Figure S13: Spatial consistency of ROIs changes in time in ABIDE data. A) Relative changes in spatial consistency between subsequent time windows. Note that the ABIDE time series are shorter than the in-house time series, which leads to a smaller number of time windows. Changes are non-random in time, similarly as in the in-house data (see Fig. 2 of the main article). The location of the nodes is determined on the same way as in Fig. 2 of the main article. B) Spatiotemporal consistency on the brain surface. Spatiotemporal consistency is anatomically non-uniformly distributed and shows strong spatial correlation. All results are averages over 28 subjects. Grayscale areas are not included in the present study (white matter and cerebellum). Note that in the ABIDE data, ROIs are on average smaller than in the in-house data and there are more voxels that do not belong to same ROI for all subjects. In the visualization, these voxels are colored with grayscale.

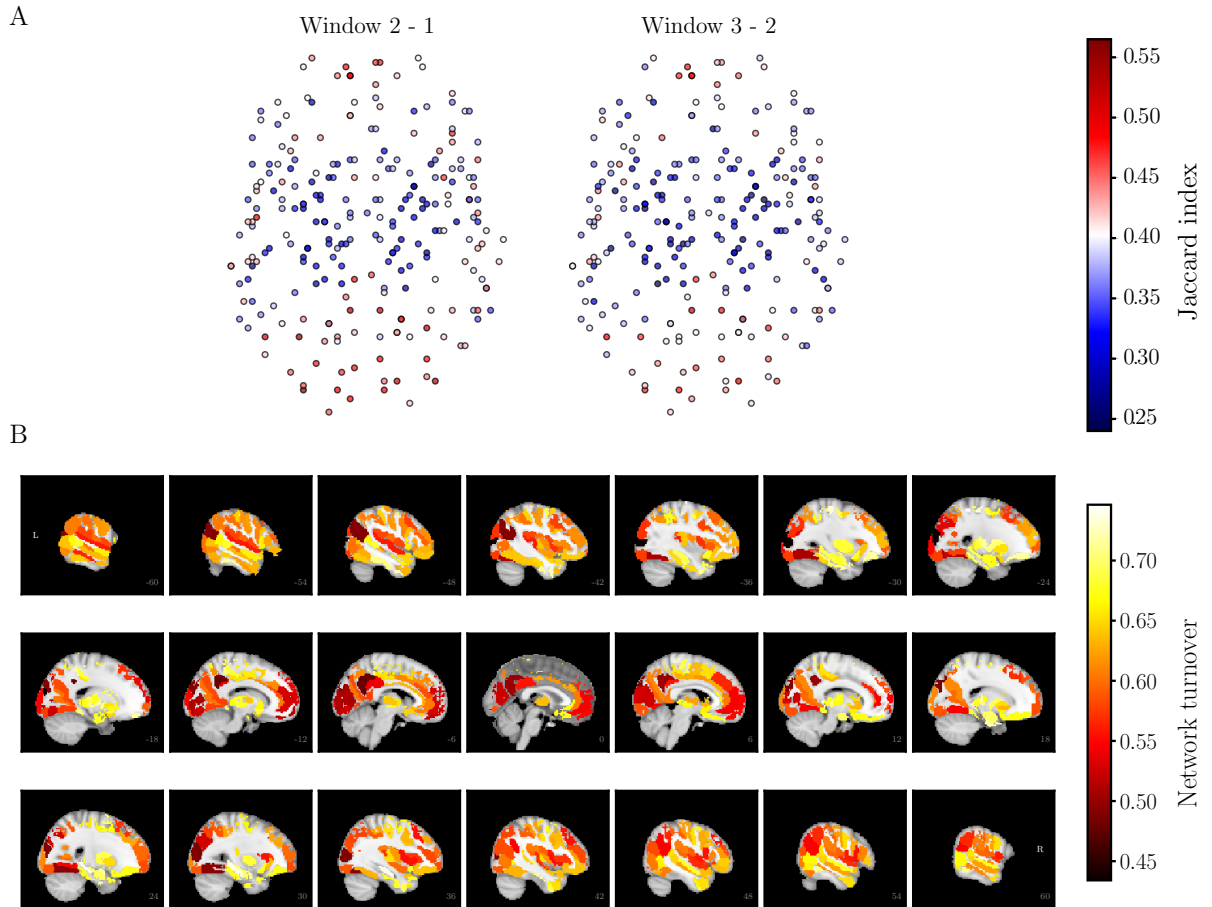


Figure S14: Significant neighborhood turnover takes place in the functional brain networks extracted from the ABIDE data. A) The Jaccard index between subsequent time windows. Values of the Jaccard index shows strong spatial correlation similarly as in the in-house data (see Fig. 3 of the main article). Node locations are defined as in Fig. 2 of the main article. B) Network turnover on the brain surface. High network turnover of subcortical areas is clearly visible. All results are averages over 28 subjects. For further details of the visualization, see Fig. S13.

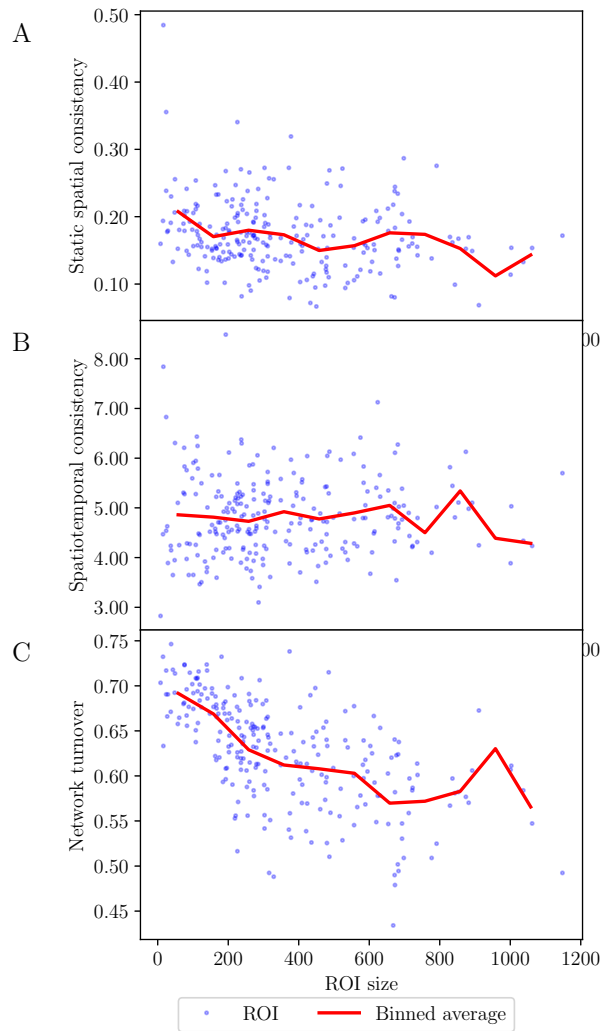


Figure S15: Relationship between the size of ROIs and their spatial and spatiotemporal consistency and network turnover in the ABIDE data. A) Static spatial consistency is negatively correlated with ROI size. B) There is no significant correlation between ROI size and spatiotemporal consistency. C) Network turnover is negatively correlated with ROI size. All results are averages over 28 subjects. The solid red lines show bin averages, binning as in Fig. 4 of the main article.

consistency and high network turnover (Fig. S16C)

With the help of PCA, we identified two groups of extreme ROIs: five ROIs with high spatiotemporal consistency and low network turnover and five ROIs with low spatiotemporal consistency and high network turnover (Fig. S17). In the ABIDE data, the first extreme group included left precuneus (4_1 and 4_4), right precuneus (4_3), left superior occipital gyrus (2_1), and right cuneus (5_3). The second extreme group contained left precentral gyrus (6_4), right striatum (6_1), left hippocampus (2_2), left inferior temporal gyrus (7_3), and right inferior temporal gyrus (7_1).

Finally, we selected four ROIs for a detailed investigation of internal connectivity. These ROIs were right precuneus (4_3), left superior occipital gyrus (2_1), left inferior temporal gyrus (7_3), and left hippocampus (2_2). The voxel-level correlation matrices of these ROIs reveal a rich internal connectivity structure (Fig. S18). Although the low-spatiotemporal-consistency ROIs and high-spatiotemporal-consistency ROIs differ from each other in terms of the overall voxel-level correlation, the internal structure is similar in all ROIs: voxels form several anticorrelated subareas. In all ROIs, this internal structure changes in time.

2.3 An alternative measure for spatiotemporal consistency

In the main article, we found a negative correlation between spatiotemporal and network turnover of a ROI. This correlation, however, strongly depends on how we define spatiotemporal consistency. The definition given in equation (3) of the main article measures stability in terms of relative change: the most stable ROIs are those that have, on average, the smallest relative change in spatial consistency. For a more complete picture, we also investigated an alternative measure of spatiotemporal consistency: the inverse of the standard deviation ($1/SD$). It quantifies stability in terms of the absolute deviation of spatial consistency from the mean over time windows. For this alternative measure, we obtained a *positive* correlation between network turnover and spatiotemporal consistency in Brainnetome ($r = 0.36, p \ll 10^{-5}$, Fig S19B) and no significant correlation in other parcellations (HO: $r = 0.14, p = 0.098$; AAL: $r = 0.11, p = 0.221$; Fig S19D, F).

At the first glance, this difference in results may look quite strange – the two measures of spatiotemporal consistency give the opposite results for the same ROIs. However, this can be understood by realizing that one of the measures is relative and the other is absolute. A ROI may show large absolute but small relative changes in spatial consistency between time windows if its spatial consistency is high on average. Indeed, those ROIs that have the highest spatiotemporal consistency in terms of relative change also have the highest static spatial consistency (Fig. 5B of the main article, Figs. S7B, S8B), which strongly correlates with the mean spatial consistency over separate time windows (Brainnetome: $r = 0.998, p \ll 10^{-5}$; HO: $r = 0.999, p \ll 10^{-5}$; AAL: $r = 0.999, p \ll 10^{-5}$). So, in summary, in ROIs with high static spatial consistency the variation of spatial consistency is absolutely large but relatively small.

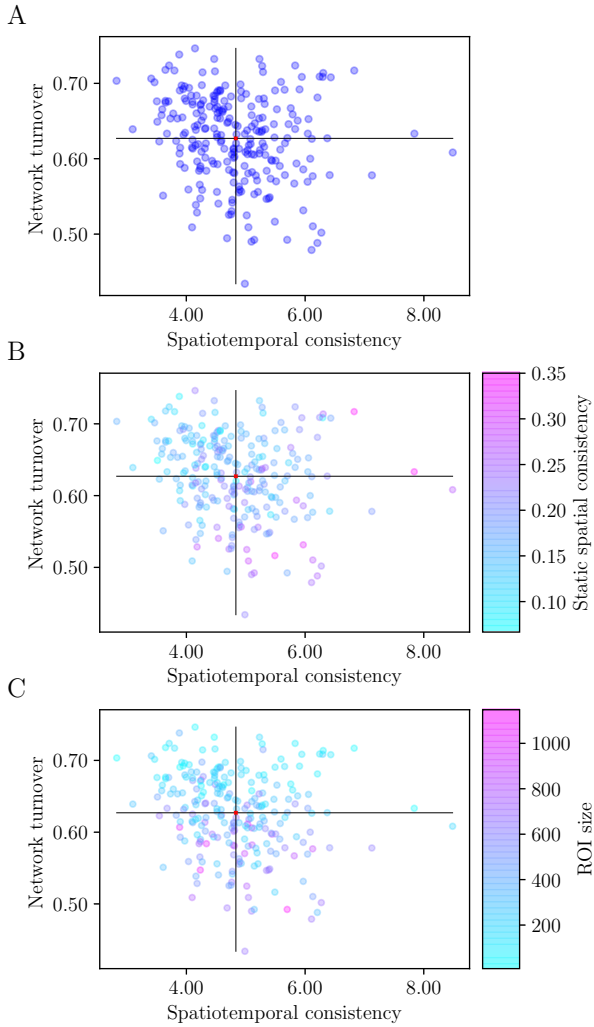


Figure S16: Relationship between static spatial consistency, spatiotemporal consistency, and network turnover in the ABIDE data. A) Spatiotemporal consistency and network turnover are negatively correlated. B) ROIs with the highest static spatial consistency tend to have also high spatiotemporal consistency and low network turnover. C) ROIs with high spatiotemporal consistency and low network turnover tend to be larger than ROIs with low spatiotemporal consistency or high network turnover. Note that unlike in Fig. 5 of the main article, here the median of spatiotemporal and network turnover over 28 subjects is visualized instead of average. For details, see the text.

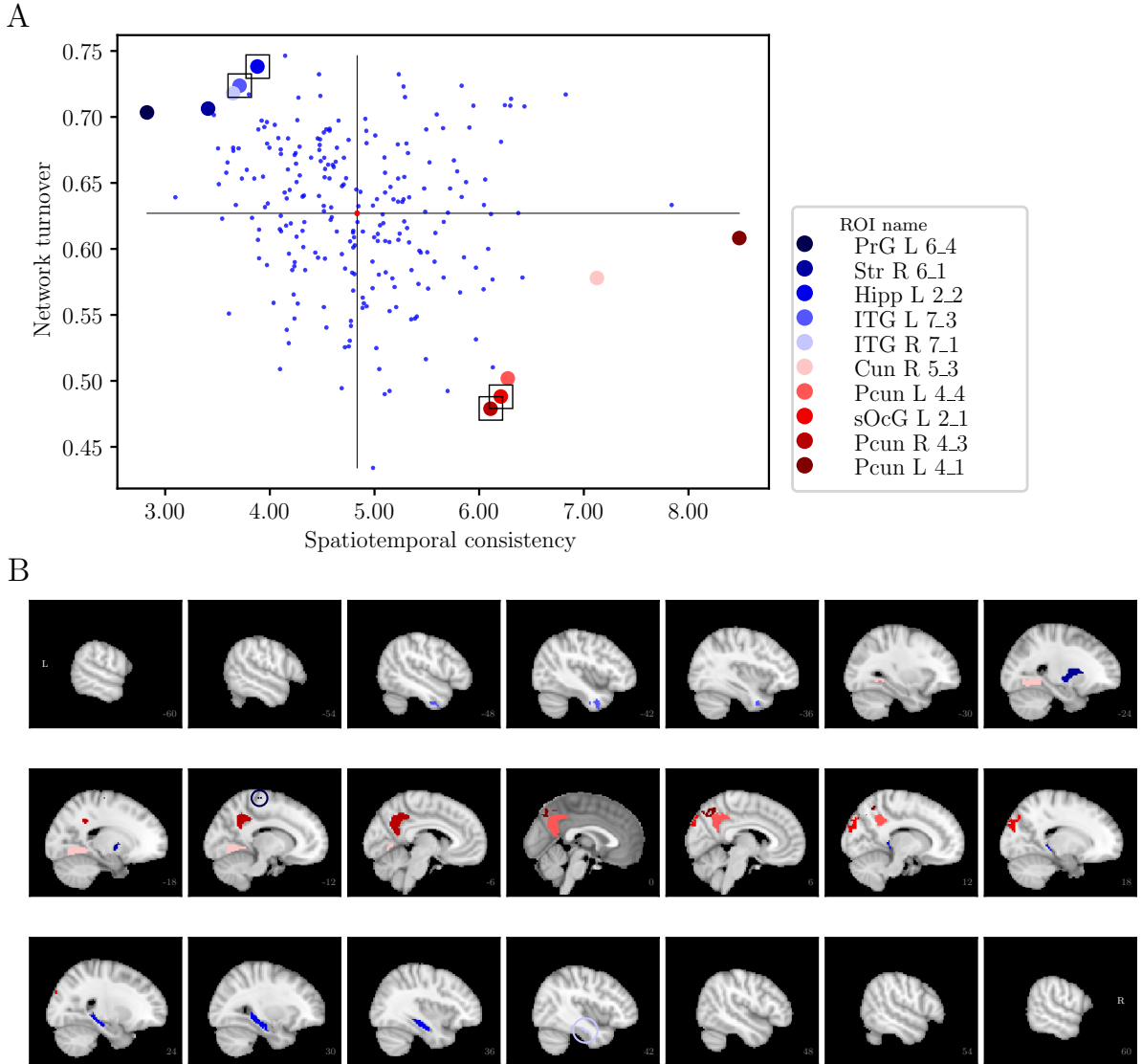


Figure S17: Extreme ROIs in terms of spatiotemporal consistency and network turnover in the ABIDE data. A) Location of extreme ROIs in the space spanned by spatiotemporal consistency and network turnover. Red ROIs have high spatiotemporal consistency and low network turnover, whereas blue ROIs have low spatiotemporal consistency and high network turnover. For further details, see Fig. 6 of the main article. B) Anatomical location of the extreme ROIs. L: left, R: right, PrG: precentral gyrus, Str: striatum, Hipp: hippocampus, ITG: inferior temporal gyrus, Cun: cuneus, Pcun: precuneus, sOcG: superior occipital gyrus

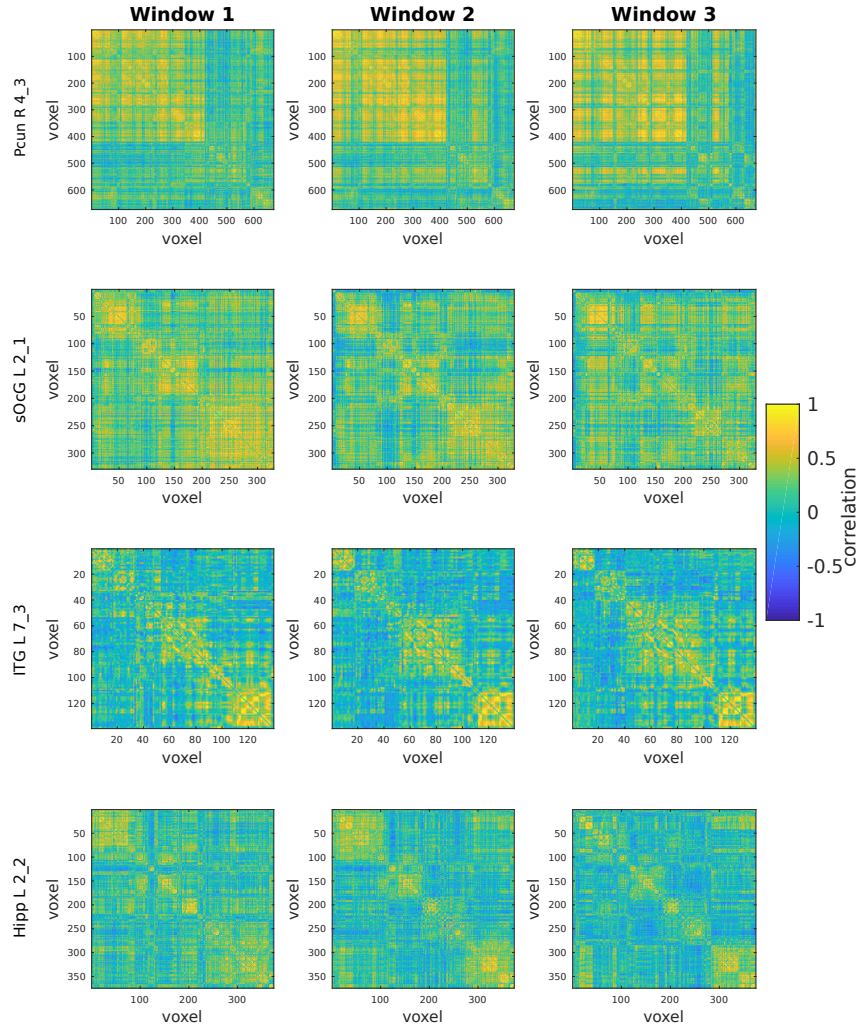


Figure S18: ROIs have rich internal connectivity structure in the ABIDE data, which is visualized by voxel-level intra-ROI correlation matrices. This structure changes in time. The upper two rows show matrices for ROIs with high spatiotemporal consistency and low network turnover, and the lower two ROIs show matrices for ROIs with low spatiotemporal consistency and high network turnover. For further details of visualization, see Fig. 7 of the main article. L: left, R: right, Pcun: precuneus, sOcG: superior occipital gyrus, ITG: inferior temporal gyrus, Hipp: hippocampus.

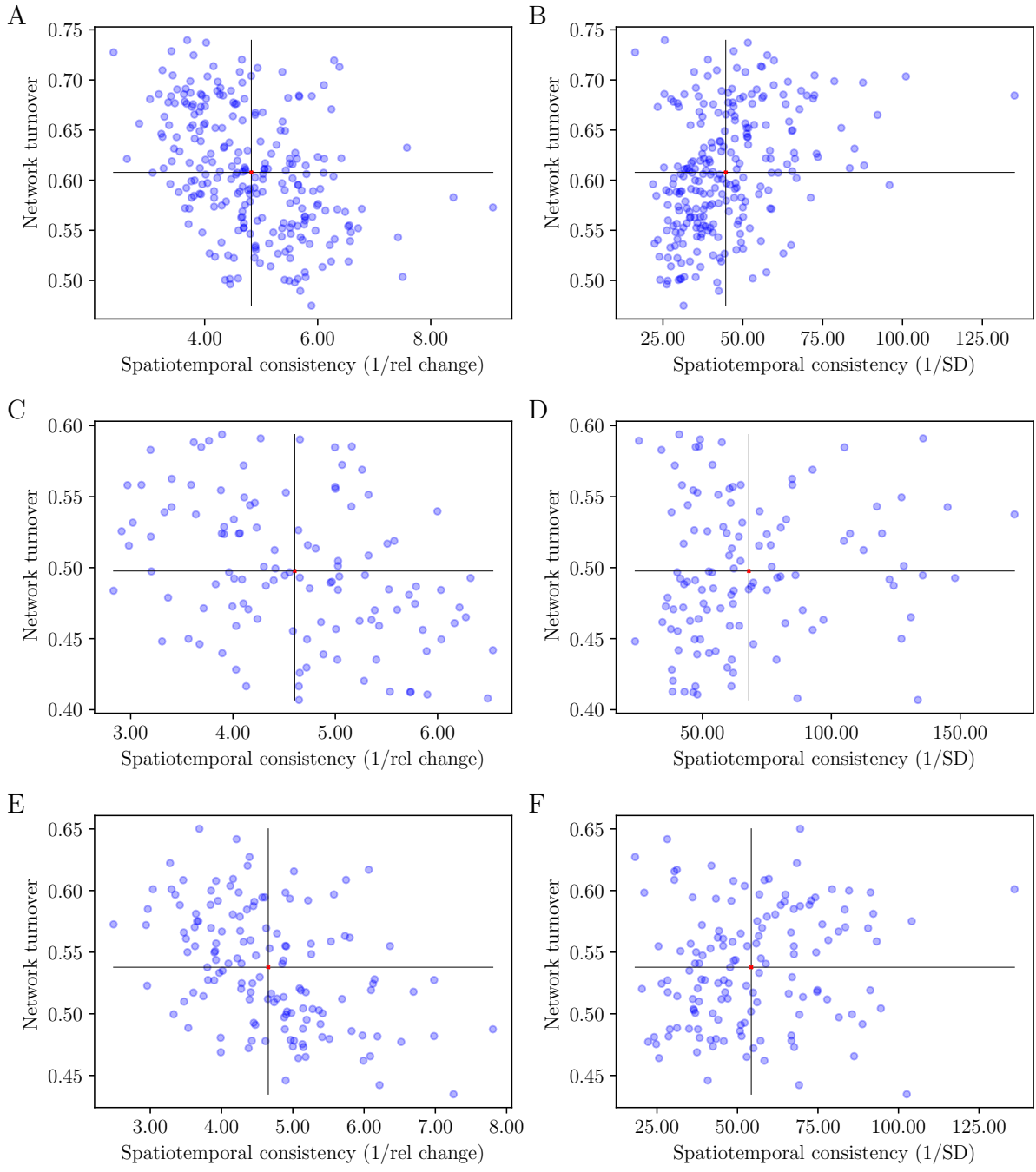


Figure S19: Definition of spatiotemporal consistency affects the relationship between spatiotemporal consistency and network turnover. When spatiotemporal consistency is defined in terms of relative change, spatiotemporal consistency and network turnover are negatively correlated in Brainnetome (A), AAL (C), and HO (E). However, an alternative definition of spatiotemporal consistency emphasizes absolute changes and leads to positive correlation in Brainnetome (B) and to no significant correlation in AAL (D) and HO (F). For discussion about differences in the two definitions of spatiotemporal consistency, see the text.

References

- Bassett, D. S., Wymbs, N. F., Porter, M. A., Mucha, P. J., Carlson, J. M., & Grafton, S. T. (2011). Dynamic reconfiguration of human brain networks during learning. *Proceedings of the National Academy of Sciences*, 108(18), 7641–7646. doi: 10.1073/pnas.1018985108
- Bassett, D. S., Wymbs, N. F., Rombach, M. P., Porter, M. A., Mucha, P. J., & Grafton, S. T. (2013). Task-based core-periphery organization of human brain dynamics. *PLoS Computational Biology*, 9(9), e1003171. doi: 10.1371/journal.pcbi.1003171
- Di Martino, A., Yan, C.-G., Li, Q., Denio, E., Castellanos, F. X., Alaerts, K., . . . Milham, M. P. (2014). The autism brain imaging data exchange: towards a large-scale evaluation of the intrinsic brain architecture in autism. *Molecular psychiatry*, 19(6), 659–667. doi: 10.1038/mp.2013.78